How Close Are Leading Tropical Tropospheric Temperature Perturbations to Those under Convective Quasi Equilibrium?

YI-XIAN LI,[a,b,c] J. DAVID NEELIN,[d] YI-HUNG KUO,[d] HUANG-HSIUNG HSU,[b,c] AND JIA-YUH YU[c]

[a] *Earth System Science, Taiwan International Graduate Program, Academia Sinica, Taipei, Taiwan*
[b] *Research Center for Environmental Changes, Academia Sinica, Taipei, Taiwan*
[c] *Department of Atmospheric Sciences, National Central University, Taoyuan, Taiwan*
[d] *Department of Atmospheric and Oceanic Sciences, University of California, Los Angeles, Los Angeles, California*

(Manuscript received 2 December 2021, in final form 25 May 2022)

ABSTRACT: In convective quasi-equilibrium theory, tropical tropospheric temperature perturbations are expected to follow vertical profiles constrained by convection, referred to as A-profiles here, often approximated by perturbations of moist adiabats. Differences between an idealized A-profile based on moist-static energy conservation and temperature perturbations derived from entraining and nonentraining parcel computations are modest under convective conditions—deep convection mostly occurs when the lower troposphere is close to saturation, thus minimizing the impact of entrainment on tropospheric temperature. Simple calculations with pseudoadiabatic perturbations about the observed profile thus provide useful baseline A-profiles. The first EOF mode of tropospheric temperature (TEOF1) from the ERA-Interim and AIRS retrievals below the level of neutral buoyancy (LNB) is compared with these A-profiles. The TEOF1 profiles with high LNB, typically above 400 hPa, yield high vertical spatial correlation (~0.9) with A-profiles, indicating that tropospheric temperature perturbations tend to be consistent with the quasi-equilibrium assumption where the environment is favorable to deep convection. Lower correlation tends to occur in regions with low climatological LNB, less favorable to deep convection. Excluding temperature profiles with low LNB significantly increases the tropical mean vertical spatial correlation. The temperature perturbations near LNB exhibit negative deviations from the A-profiles—the convective cold-top phenomenon—with greater deviation for higher LNB. In regions with lower correlation, the deviation from A-profile shows an S-like shape beneath 600 hPa, usually accompanied by a drier lower troposphere. These findings are robust across a wide range of time scales from daily to monthly, although the vertical spatial correlation and TEOF1 explained variance tend to decrease on short time scales.

KEYWORDS: Convection; Thermodynamics; Tropical variability; Temperature; Troposphere; Empirical orthogonal functions

1. Introduction

The theory of convective quasi equilibrium (CQE) is essential for our understanding of the interaction between moist convection and the large-scale environment in the tropics (Emanuel et al. 1994; Neelin et al. 2008; Raymond and Herman 2011; Yano and Plant 2012, 2016). The CQE concept was first proposed by Arakawa and Schubert (1974) in which the conditional instability generated by the large-scale forcing is assumed to be consumed by cloud-scale convective processes. It helps explain why the environmental temperature profile is constrained toward moist adiabats, as seen in observations (Betts 1982; Xu and Emanuel 1989; Brown and Bretherton 1997; Holloway and Neelin 2007; Nie et al. 2010). Multiple convective parameterizations that adjust the environmental temperature toward the expected profiles have been used in climate models [e.g., Manabe et al. 1965; Kuo 1974; Betts 1986; see also Arakawa (2004) for a comprehensive review] and an intermediate-complexity model of tropical circulation has been derived using the theoretical temperature structure (Neelin and Yu 1994; Neelin and Zeng 2000; Sobel and Neelin 2006).

Following the CQE assumption, Yu and Neelin (1997) derived a theoretical profile of temperature variations—borrowing from the notation therein, we refer to such vertical profiles of temperature perturbations constrained by convection as A-profiles hereafter. Given a typical tropical temperature sounding, the corresponding A-profile increases gradually with height, reaches its peak value around 225 hPa, and decreases with further increase in height. Such a structure is consistent with the observed leading mode of temperature variation (Holloway and Neelin 2007; Lin et al. 2015). In the context of global warming, observational and modeling work has also noted a signal with amplified upper-tropospheric warming that exhibits a structure similar to the A-profile (Santer et al. 2005; O'Gorman and Singh 2013; Fueglistaler et al. 2015; Steiner et al. 2020).

In the tropics, low values of the Coriolis force allow propagating gravity waves to effectively adjust horizontal temperature variation toward a weak temperature gradient (WTG) state (Neelin and Held 1987; Sobel et al. 2001; Bretherton and Sobel 2003; Kuang 2008). One thus expects that temperature

Denotes content that is immediately available upon publication as open access.

Supplemental information related to this paper is available at the Journals Online website: https://doi.org/10.1175/JAS-D-21-0315.s1.

Corresponding author: Jia-Yuh Yu, jiayuh@atm.ncu.edu.tw

DOI: 10.1175/JAS-D-21-0315.1

profiles in deep-convective clouds—dictated by moist adiabats, potentially modified by entrainment—can impact the large-scale surroundings (Singh and O'Gorman 2013), and that the tropical temperature exhibits a horizontal pattern much broader than that of deep convection. Previous studies mostly focused on examining the leading mode of temperature variation in comparison to the theoretical profile but without investigating the geographical pattern. This manuscript intends to address the geographical pattern of tropospheric temperature profile, and whether the theoretical A-profile provides a reasonable approximation to the leading structure of temperature variations. A useful indicator of this typical vertical structure is the shape captured by the first EOF mode of temperature, denoted by TEOF1 hereafter (discussion of TEOF1 shape compared to profile perturbations and of the variance captured by this structure will be addressed in sections 3 and 5, respectively).

Another factor expected to impact temperature variation is the depth of convection, which depends on the large-scale environment. Using the level of neutral buoyancy (LNB) as a proxy for convection depth, we also examine the dependence of the leading mode of temperature variation (i.e., TEOF1) in the tropics on LNB. In particular, whether the occurrence of low LNB (or conditions unfavorable to deep convection) can affect the temperature variation will be tested.

In tropical regions where WTG is robust, the A-profile serves as a useful proxy to provide a corresponding in-cloud profile of temperature perturbation constrained by deep convection. However, typical derivations of the A-profile make use of moist adiabatic assumptions without including entrainment. Recent observational and computational evidence has pointed to substantial entrainment throughout the lowest few kilometers (Siebesma et al. 2003; Schiro et al. 2018; Savazzi et al. 2021). It is important to ask how the A-profile characterizing perturbations of convective plume temperatures is modified when entrainment is considered, and to what extent the moist adiabatic approximation might still be useful. Therefore, we compare the temperature perturbations of in-cloud temperature approximated by entraining and nonentraining plume calculations for deep-convective conditions and the corresponding A-profile.

Note that while CQE posits that convection tends to adjust temperature profiles on fairly short time scales, recent work suggests this adjustment coexists with substantial variations about the CQE point. Indications of the probability distribution of such variations in moisture–temperature or estimated buoyancy variables can be seen for instance in Kuo et al. (2018), Ahmed and Neelin (2018), and Adames et al. (2021). There would be multiple sources of the variability, e.g., associated with the adjustment process, with differential effects in the boundary layer versus free troposphere, with wave variability interacting with convection at multiple time scales that are not in perfect CQE, with variations that are not convective or have not yet begun to convect. We thus anticipate that the fraction of temperature variability explained by CQE may be reduced at shorter time scales. Here, we focus on the extent to which the vertical structure of the typical temperature profile that can be explained by CQE.

This manuscript is organized as follows. Section 2 describes the data and the methodology used here. Section 3 shows the vertical structure of the A-profile via PDF and the associated sensitivity test to entrainment assumptions. Section 4 displays the geographical patterns of the climatological LNB and A-profile. Section 5 compares the observational leading mode and the corresponding theoretical A-profile in the vertical. Section 6 examines maps of vertical spatial correlation between the leading mode and A-profile with prescribed or LNB-based upper boundaries of the EOF calculation. Section 7 presents the change of correlation when excluding low-LNB instances (note that all correlations discussed in the text are vertical spatial correlations). Discussion and conclusions are given in section 8.

2. Data and methodology

a. Datasets

The evaluation of the TEOF1 uses the data of atmospheric temperature T. Our analysis also requires the LNB, which depends on geopotential height Z and specific humidity q. Here, we use the data from the daily and monthly ERA-Interim products (Dee et al. 2011) and the AIRS/*Aqua* L3 daily and monthly standard physical retrieval (AIRS+AMSU) 1° × 1° V006 (AIRX3STD and AIRX3STM; AIRS Science Team and Teixeira 2013a,b; AIRS hereafter). For conditioning temperature profiles on convection, we adopt the precipitation from ERA-Interim and the supporting AIRX3SPD and AIRX3SPM products for AIRS (AIRS Science Team and Teixeira 2013c,d). The 3B43 monthly rainfall data from TRMM (Huffman et al. 2007, 2010) are also used to compute the precipitation climatology. Given that CQE is most relevant for the tropical atmosphere, and to avoid the influence of surface terrain, we restrict our analysis to tropical ocean between 30°S and 30°N. We use data for the period of 2003–15 covering most of AIRS records. Prior to analysis, the ERA-Interim data are coarse grained to match the 1° × 1° grid of AIRS data.

b. Theoretical A-profile

The CQE theory assumes that the temperature variations in the tropical atmosphere are constrained by moist convection, leading to a particular structure of tropospheric temperature variations which we refer to as the A-profile. We use this term in general for the profile toward which the convection adjusts, which may include entrainment or other effects. However, the simplest case is based on moist adiabatic assumptions. For this, we follow a simple construction of the A-profile documented in Yu and Neelin (1997) based on the saturation moist static energy (MSE), ignoring effects of entrainment on parcel perturbations. The derivation is briefly outlined below.

Consider the saturation MSE

$$h_s \equiv s + l_v q_s = c_{pd} T + gZ + l_v q_s, \tag{1}$$

where $s \equiv c_{pd}T + gZ$ is the dry static energy, $q_s(T, p)$ the saturation specific humidity with respect to liquid water, Z the geopotential height, $c_{\mathrm{pd}} = 1004\ \mathrm{J\ kg^{-1}\ K^{-1}}$ the specific heat

of dry air at constant pressure, and $l_v = 2.5 \times 10^6$ J kg^{-1} the latent heat of vaporization.

Inside deep-convective clouds, one expects the temperature to locally follow moist adiabats (dry adiabats below the LCL)—conserving h_s under the hydrostatic assumption. At low latitudes where the Coriolis force is weak, the large-scale environmental temperature is effectively adjusted via propagating waves in response to convective heating (Neelin and Held 1987; Sobel et al. 2001; Bretherton and Sobel 2003). Therefore, under the constant influence of deep convection, simple forms of CQE omitting entrainment postulate that the tropospheric temperatures relative to climatological mean can be approximated by perturbations of moist adiabats, i.e.,

$$\frac{dh_s'}{dp} = 0. \tag{2}$$

Here we denote the deviation from climatology (overbar) using a prime, and

$$T = \overline{T} + T',$$

$$h_s' = h_s(T) - h_s(\overline{T}). \tag{3}$$

Using hydrostatic approximation, ideal gas law, and Clausius–Clapeyron relation,

$$h_s' \approx c_{pd}T' + R_d\int_p^{p_0}\frac{T'(p')}{p'}dp' + l_v\frac{\varepsilon}{p}\frac{de_s}{dT}T'$$

$$= c_{pd}(1+\gamma)T' + R_d\int_p^{p_0}\frac{T'(p')}{p'}dp', \tag{4}$$

where $p_0 \equiv 1000$ hPa is a reference pressure, $\varepsilon \equiv R_d/R_v = 0.622$ the ratio of the gas constant for dry air to that of water vapor, e_s the saturation vapor pressure with respect to liquid, and $\gamma \equiv \varepsilon e_s l_v^2/(c_{pd}pR_vT^2)$.

Substituting Eq. (4) into Eq. (2), one can derive

$$c_{pd}\frac{d[(1+\gamma)T']}{dp} = R_d\frac{T'}{p}.$$

Dividing both sides by $c_{pd}(1+\gamma)T'$ and integrating from $p_{\rm LCL}$ upward to p yield (with $\kappa \equiv R_d/c_{pd}$)

$$\frac{\{1+\gamma[T(p)]\}T'(p)}{\{1+\gamma[T(p_{\rm LCL})]\}T'(p_{\rm LCL})} = \exp\int_{p_{\rm LCL}}^{p}\frac{\kappa}{1+\gamma[T(p')]}d\ln p'$$

or

$$\frac{T'(p)}{T'(p_{\rm LCL})} = \frac{1+\gamma[T(p_{\rm LCL})]}{1+\gamma[T(p)]}\exp\left\{-\kappa\int_p^{p_{\rm LCL}}\frac{1}{1+\gamma[T(p')]}d\ln p'\right\}, \tag{5}$$

i.e., the temperature perturbation structure, normalized at LCL, can be determined given atmospheric temperature. Below the LCL, the dry static energy s is used instead of h_s, i.e., dropping the γ terms in Eq. (5) for $p > p_{\rm LCL}$. Note that for $p_s > p_{\rm LCL}$, $ds'/dp = 0$ implies $(p_{\rm LCL}/1000\,{\rm hPa})^\kappa = T'(p_{\rm LCL})/T'(p_0)$. Thus, for each sounding, we define its corresponding A-profile by

$$A[p,T(p)] \equiv \frac{T'(p)}{T'(p_0)} = \left(\frac{p_{\rm LCL}}{1000\ {\rm hPa}}\right)^\kappa\frac{1+\gamma[T(p_{\rm LCL})]}{1+\gamma[T(p)]}$$

$$\exp\left\{-\kappa\int_p^{p_{\rm LCL}}\frac{1}{1+\gamma[T(p')]}d\ln p'\right\}, \quad p \le p_{\rm LCL}, \tag{6}$$

and

$$A[p,T(p)] \equiv \left(\frac{p}{1000\ {\rm hPa}}\right)^\kappa, \quad p > p_{\rm LCL}. \tag{7}$$

Equations (6) and (7) require knowledge of the LCL, hence the temperature and specific humidity at $p_0 \equiv 1000$ hPa (for simplicity, we assume that parcels originate from this level). Individual A-profiles are calculated via Eqs. (6) and (7) with soundings from the ERA-Interim and AIRS data interpolated to a 5-hPa grid. Experiments with a fixed LCL at 950 hPa indicate that the A-profiles are not sensitive to LCL (not shown).

Equations (6) and (7) provide a quantitative description of this A-profile. It is worth noting that the evaluation of this approximation for the A-profile does not make use of a mean state, although the temperature perturbation is defined relative to a certain mean. It does not assume the tropospheric temperature to be completely moist adiabatic, but uses the moist adiabatic assumptions for perturbations relative to the local temperature profile.

c. Level of neutral buoyancy

The LNB provides a useful proxy for the depth of convection. This work also examines the sensitivity of temperature variation to the depth of convection. In this manuscript, LNB is determined as follows. Consider a parcel adiabatically lifted upward from 1000 hPa while conserving its moist static energy $h \equiv c_{pd}T + gZ + l_vq$. We find the level—presumably in the upper troposphere—at which the environmental h_s first exceeds the 1000-hPa value of h and call it LNB. Note that LNB does not necessarily exist when the near-surface h is smaller than the value of tropospheric h_s. For consistency with the pseudoadiabatic calculation, virtual temperature effects are neglected. Entrainment is also omitted in this calculation, since we are looking for an estimator of the high end of the depth of convection.

d. Leading EOF mode of observed temperature variation

We compute the TEOF1 via covariance matrix using the daily, pentadly, and monthly mean temperature profiles (pentadly derived from daily data). An EOF requires anomalies as input. Here, to remove the seasonal cycle, at each geographical location and level, we subtract the multiyear mean (climatology) of each day, pentad, and month for each temperature profile. These profiles of temperature anomalies will then be calculated for the EOF as the input.

As the EOF requires specifying a range of analysis in the vertical, we compute the TEOF1 in $[p_{\rm eof}, 1000\ {\rm hPa}]$, where

p_{eof} is either prescribed or determined by the climatological value of LNB. To examine the extent to which the leading EOF structure can be considered representative, we also carried out alternate analysis of the structure, including median and interquartile range examined in Fig. 1, regressions on the vertical mean temperature in the free troposphere, and analysis of the variance captured by EOF1 as discussed in the appropriate sections below. In each case the structure of TEOF1 was found to be representative of the structure to a good approximation.

e. *Entrainment assumptions and plume temperature variation*

To test how the entrainment assumptions inside convective updrafts impact the temperature structure, we also compute quartiles of the plume temperature profiles with entrainment assumptions in the no-mixing and deep-inflow-B (DIB) schemes used in Holloway and Neelin (2009), as outlined below.

Total water specific humidity (q_t) and ice–liquid water potential temperature (θ_{il}), derived from input temperature and specific humidity, in a hypothetical parcel raised from 1000 hPa are conserved without entrainment in the no-mixing scheme. The DIB uses an idealized updraft vertical velocity profile (a quarter sine wave between 1000 and 430 hPa; Holloway and Neelin 2009) to compute mixing coefficients as the magnitude of entrainment, neglecting detrainment (above 430 hPa, where the mass flux no longer increases, entrainment is set to zero for simplicity). In both cases, condensate can form when the parcel is saturated, either liquid or ice depending on the plume temperature (above or below 0°C), and for approximate consistency with the pseudoadiabatic A-profile calculation all condensate is removed immediately after formation. Plume temperature is then calculated by converting q_t and θ_{il} (after mixing with the environment for DIB) at 5-hPa levels. The steps of computing the quartiles are described below.

First, we follow Holloway and Neelin (2009) and compute the plume temperature profiles using the daily environment temperature and humidity data with the DIB and no-mixing assumptions on the entrainment. Next, we compute the monthly mean of the entraining plume temperature profiles conditioned on precipitation. Because convective events with substantial precipitation are the main source of gravity waves that adjust temperature structure in the tropics, only those instances with daily precipitation exceeding 5 mm are considered here for the conditional monthly mean at each geographic location. We then compute the perturbations by subtracting plume temperatures from the multiyear mean at each level and normalize all the perturbation profiles to have the same root-mean-square as the corresponding conditionally averaged A-profile. Last, we calculate three quartiles (25th percentile, median, 75th percentile) of the normalized perturbations at each level to present the middle half of the distribution.

3. A-profile and sensitivity of temperature structure to entrainment assumptions

To give a sense of the typical behavior of A-profile, at each geographic location, we compute the A-profiles by substituting the ERA-Interim and AIRS monthly mean temperature profiles into Eqs. (6) and (7), and compute the time-mean of the A-profiles. The PDF of these mean A-profiles over tropical ocean are displayed in Figs. 1a and 1b as a function of vertical level (gray shading), with the yellow lines indicating the overall average A-profiles. The PDFs computed using daily mean temperature exhibit a similar pattern (not shown).

In Figs. 1a and 1b, the value of A-profile increases from unity at 1000 hPa, reaching its peak near 225 hPa and starting to decrease with further increase in height. The average A-profile (yellow line) tends to follow the most probable values throughout the troposphere except for near 225 hPa, where the average is slightly smaller than the most probable value. The top-heavy structure of the A-profile shown here is consistent with the tropical tropospheric temperature perturbations in prior studies (e.g., Holloway and Neelin 2007; O'Gorman and Singh 2013).

The average A-profiles (yellow lines) in Figs. 1a and 1b are replicated in Figs. 1c and 1d, together with the average A-profiles conditioned on daily precipitation exceeding 5 mm (red lines), indicative of deep convection. These two profiles exhibit similar behavior—excluding events with low or no precipitation from the computation of average A-profiles do not greatly impact the outcome. That the A-profiles under various conditions presented here exhibit similar structures is consistent with weak temperature gradient in the tropics associated with low values of the Coriolis force, allowing deep convection to effectively adjust the large-scale tropospheric temperature, even at a distance away from precipitation.

Given that in-cloud temperature structures can affect the large-scale temperature, and that entraining plume calculations provide reasonable approximations to in-cloud temperatures (Singh and O'Gorman 2013; Singh et al. 2019), one might wonder how the entertainment assumptions adopted by plume calculations affect the resulting temperature structure. This is demonstrated by the solid and dashed black lines in Figs. 1c and 1d, which represent the medians of the normalized plume temperature perturbations (scaled to have the same root-mean-square as A-profile) computed over days with daily precipitation exceeding 5 mm, with interquartile ranges shown in light and dark gray shadings with DIB (i.e., heavy entrainment in the lower troposphere) and no-mixing entrainment assumptions, respectively. The medians from plume calculations using the DIB and no-mixing assumptions are both similar to the theoretical A-profiles, with vertical spatial correlation coefficients exceeding 0.96 and 0.98, respectively. The interquartile ranges with DIB assumption tend to be larger than those with no-mixing assumption, especially in the lower troposphere. These occur for a simple reason: the convection and hence precipitation occurs only when the lower troposphere is relatively close to saturation. Although the entrainment can yield large differences in the plume profile for a dry lower troposphere, when the air is close to saturation, the difference between plume profiles is only modestly affected. Departures from the A-profiles can be noted. The interquartile ranges exhibit larger spread in the boundary layer below ~900 hPa (relative to upper levels),

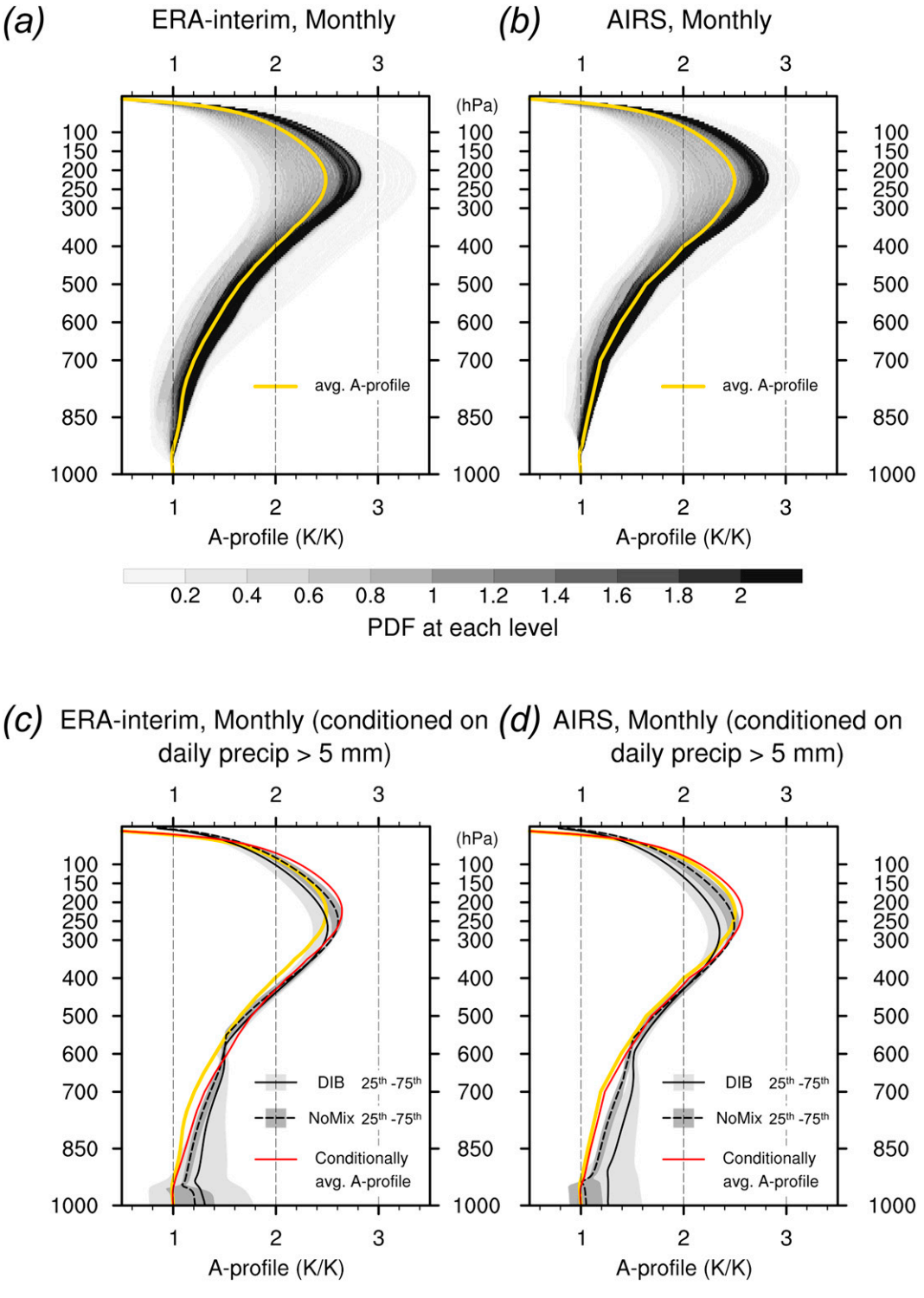

FIG. 1. (a) PDF (color shading; dimensionless) of tropical A-profile value $T'(p)/T'(1000\ \text{hPa})$ at each level computed using ERA-Interim monthly data. The yellow solid line represents the averaged A-profile. (b) As in (a), but using AIRS monthly data. (c) Average A-profile (red) and medians of DIB (solid black) and no-mixing (dashed black) normalized plume temperature perturbations computed with ERA-Interim monthly data, all conditioned on ERA-Interim daily precipitation exceeding 5 mm. The median profiles are normalized to have the same root-mean-square as the A-profile. Interquartile ranges of normalized plume temperature perturbations for DIB (light gray shading) and no-mixing (dark gray shading) are also shown. (d) As in (c), but replacing the ERA-Interim data with AIRS data. The yellow lines in (a) and (b) are replicated in (c) and (d).

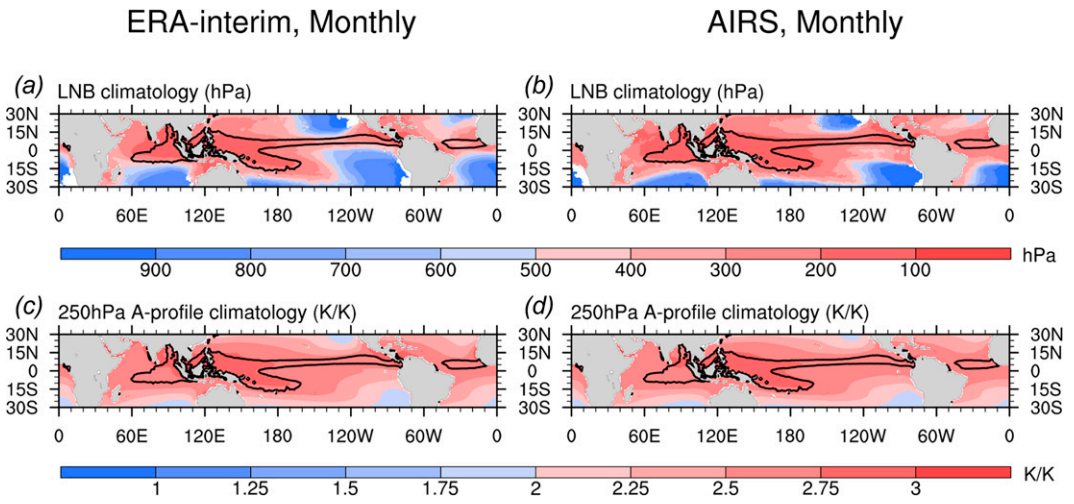

FIG. 2. (a) 5 mm day^{-1} climatological precipitation from TRMM 3B43 data (black contours) and climatology of level of neutral buoyancy (LNB; color shading) estimated with ERA-Interim monthly data. (b) As in (a), but replacing ERA-Interim with AIRS monthly data. (c) Climatology of 250-hPa A-profile computed with ERA-Interim monthly data. (d) As in (c), but with AIRS monthly data. The black contours in (a) are replicated in (b)–(d).

coinciding with typical LCL height. Such effects can be reproduced in plume computations with varying LCL heights.

Here are some differences between the profiles computed as the medians of the temperature perturbations from the plume computations and the theoretical averaged A-profile: at the top of the boundary layer variations in the LCL create a kink in the plume profiles, while the theoretical A-profile computed analytically for small perturbations is less affected by LCL variations; in the upper troposphere the theoretical A-profile ignores the latent heat of freezing; finally, the changes in shape create slight differences throughout the profile due to normalization. However, the entrainment itself is producing little difference in profile shape (solid black versus dashed black lines in Figs. 1c,d), relative to the variations in amplitude of the A-profile in Figs. 1a and 1b. This justifies the use of A-profile based on the moist adiabat for many purposes even though the atmosphere has high entrainment—the effect of entrainment is strong, but it acts principally to prevent convection until the lower troposphere is sufficiently saturated (Derbyshire et al. 2004; Holloway and Neelin 2010; Sahany et al. 2012; Kuo et al. 2017) whereupon it has little impact on the temperature profile. For simplicity we will use the pseudoadiabatic A-profile for reference in comparison to the observed temperature variations hereafter.

4. Climatologies of level of neutral buoyancy and A-profile

In examining vertical temperature profiles across the tropics, the depth of convection will have a substantial impact on the depth through which we expect profiles typical of convection to be relevant. We thus examine the spatial dependence of the LNB as a proxy for the depth of convection. Spatial variations in the amplitude of the A-profile are useful for comparison.

Figures 2a and 2b show the climatology of the LNB estimated with the ERA-Interim and AIRS monthly data. The 5 mm day^{-1} contours (black) of climatological precipitation from the TRMM 3B43 data are overlaid for comparison. The precipitation contours mark regions of high occurrence of deep convection. The LNB climatology exhibits a geographic pattern similar to that of the precipitation contour since deep convection tends to produce much more precipitation in the tropics. Minor departures from the precipitation contour can be noted along the convective margins.

Figures 2c and 2d display the 250-hPa A-profile climatology (color shading) together with the precipitation contours. The A-profile, i.e., the theoretical tropospheric temperature perturbation exhibits a broader spatial pattern compared with that of the LNB and precipitation—temperature perturbations originating from deep convection tend to spread across wider spatial scales in the tropics due to gravity wave propagation.

5. Leading mode of tropospheric temperature perturbation approximated by A-profile

Results in Fig. 2 are consistent with the expectation that tropospheric temperatures tend to exhibit a broader pattern than that of the occurrence of convection in the tropics. It should be noted, however, that the A-profile is a postulated theoretical approximation to tropospheric temperature perturbation, and does not necessarily represent the actual temperature structure. In this section, we directly compare the leading mode of tropospheric temperature perturbation to the A-profile, and examine their relationship to the LNB.

In Figs. 3a–g, the climatological monthly mean A-profile (dashed) and TEOF1s (solid lines) are displayed for different values of LNB (gray shading; divided into 7 bins). Here, the TEOF1s and LNB are computed using the monthly (blue),

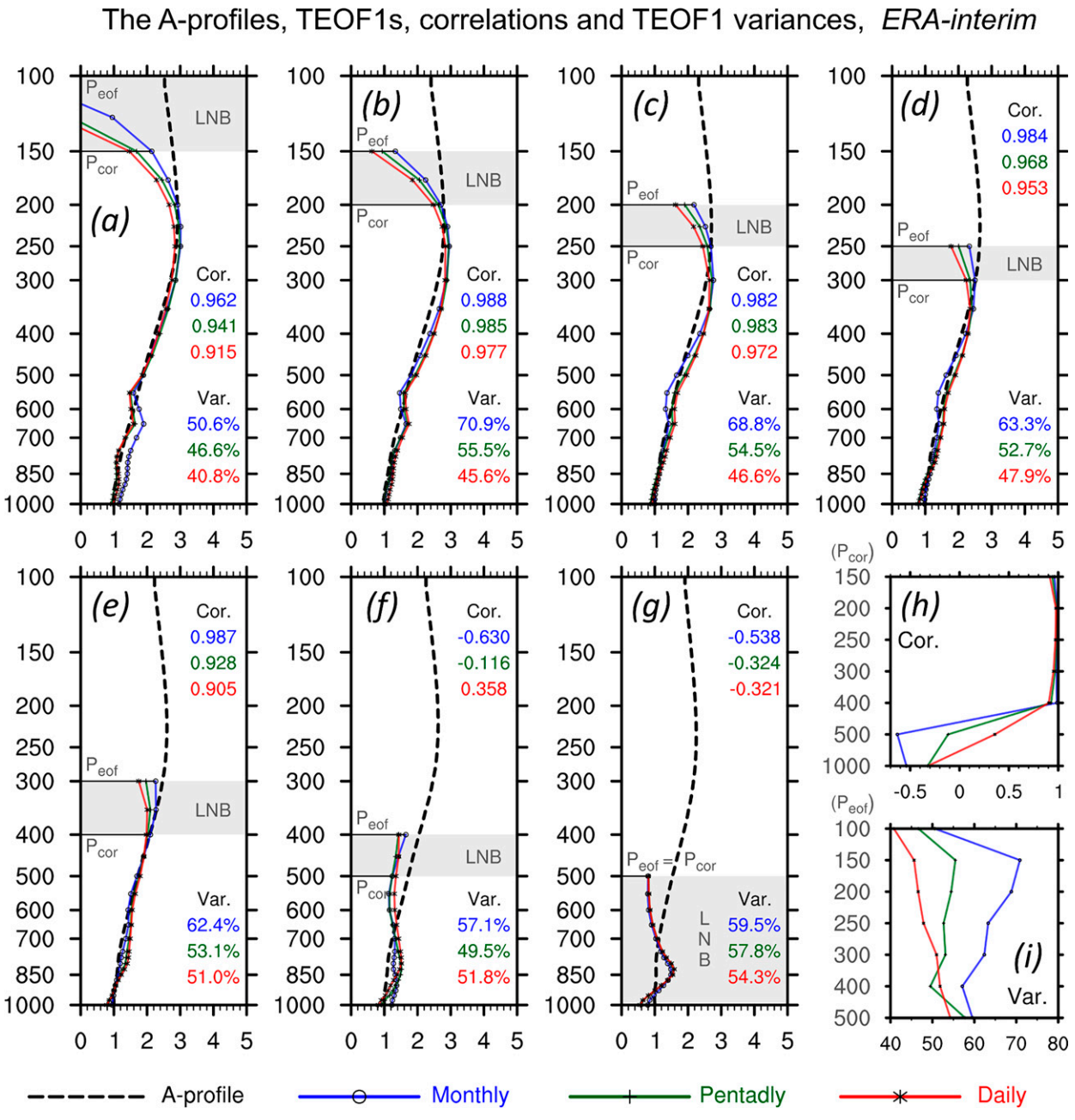

FIG. 3. (a) A-profile (dashed) averaged over all monthly mean A-profiles with 150 ≥ LNB > 100 hPa (gray shading) and TEOF1 computed over [p_{eof}, 1000 hPa] from all such instances using monthly (blue), pentadly (green), and daily (red) ERA-Interim data. The variances explained by TEOF1s and their vertical spatial correlation coefficients with the mean A-profile in [p_{cor}, 1000 hPa] are also listed. (b)–(g) As in (a), but for different LNB range, p_{eof}, and p_{cor}. (h) Vertical spatial correlation coefficients and (i) variances explained by TEOF1s from (a) to (g).

pentadly (green), and daily (red) mean temperatures. The vertical spatial correlations between the TEOF1s and A-profiles and the variances explained by TEOF1s are also shown for reference. The p_{eof}, as the upper boundary of the EOF analysis determined by the upper edge of the LNB bins, is used as a proxy of convection depth. It is useful to define a separate upper boundary of the vertical range of calculating correlation between the A-profile and the TEOF1s, p_{cor}. This allows the TEOF1s to capture a deeper temperature response while avoiding taking temperature structure beyond the convection depth into the quantification of correlation. Here we use the lower edge of the LNB bins as p_{cor}.

When the LNB is high enough (e.g., Figs. 3a–e), the TEOF1s tend to coincide with the A-profiles through much of

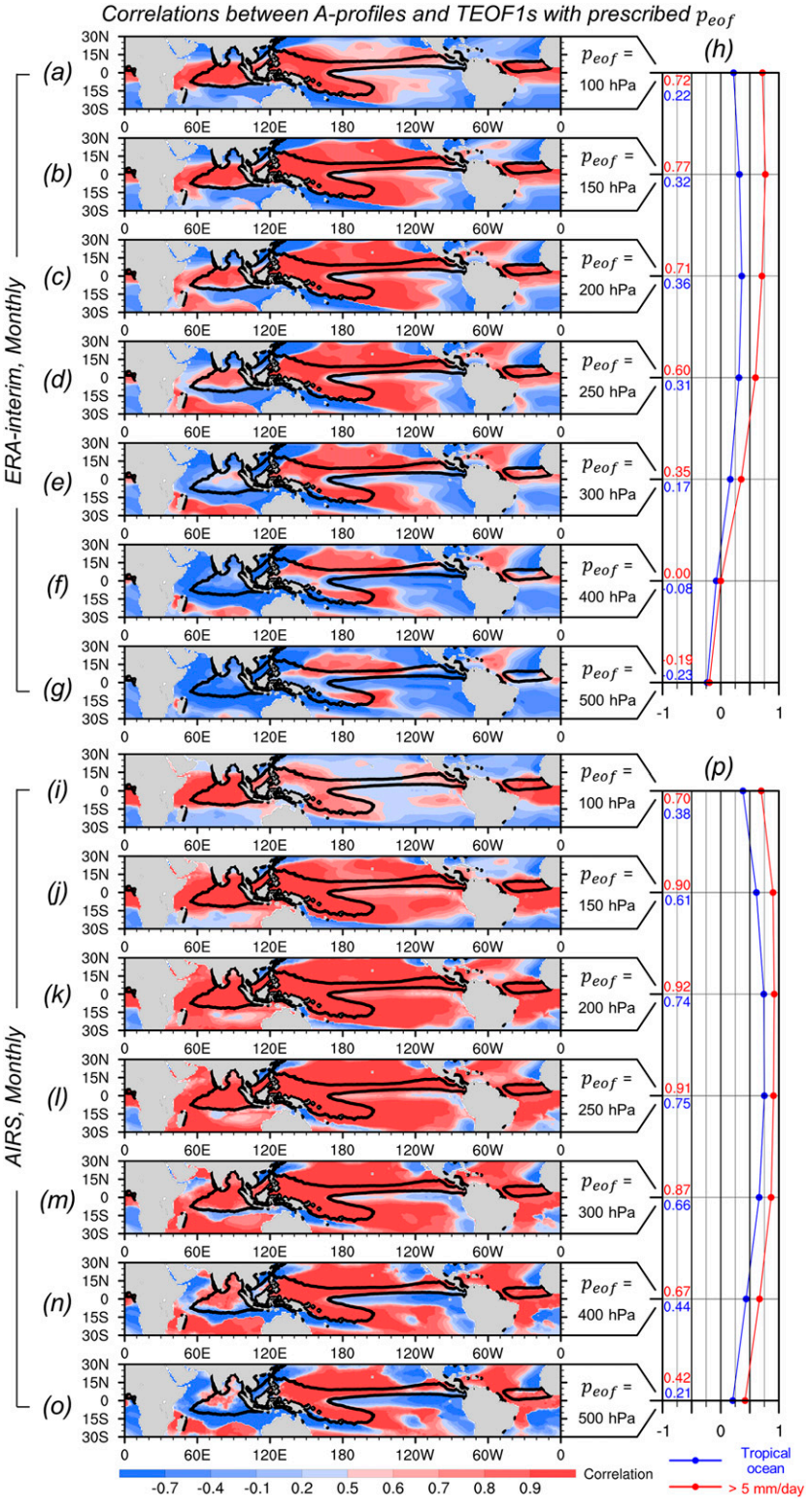

FIG. 4. (a) Vertical spatial correlations (color shading) between the climatological monthly mean A-profile and TEOF1 in [1000 hPa, p_{eof} = 100 hPa] over tropical ocean for ERA-Interim monthly data. The black contours mark the 5 mm day^{-1} climatological precipitation from TRMM 3B43 data. (b)–(g) As in (a), but with different p_{eof} values. (h) Mean vertical spatial correlations averaged over tropical ocean (blue) and within the 5 mm day^{-1} precipitation contours (red) for (a)–(g). (i)–(p) As in (a)–(h), but using AIRS monthly data. Here the precipitation is from the TRMM 3B43 data.

the depth of the convection. This yields correlations over [p_{cor}, 1000 hPa] exceeding 0.9 (the correlation as a function of p_{eof} is summarized in Fig. 3h). Substantial negative deviations of the TEOF1s from the A-profiles can be seen near the LNB—a feature known as the convective cold top (Holloway and Neelin 2007). Thus, the theoretical A-profile provides a reasonable approximation to the leading mode of tropospheric temperature perturbation when LNB is higher than 400 hPa, i.e., in regions favorable to deep convection. The cold-top feature occurs at a height varying with the LNB. We note that a nonentraining LNB estimate is used here, but it appears to be a plausible estimator of where the actual profile deviates from the A-profile. We hypothesize that this occurs for the same reasons outlined in section 3: convection only occurs once the profile is sufficiently moist. The cold-top deviations suggest that there are important processes not considered in the A-profile derivation. While it is beyond the scope of this study to pursue a theoretical derivation, we suggest that it involves the matching of a wave dynamics solution above the convective heating with the quasi-equilibrium constraints occurring below the cloud top.

For low LNB in Figs. 3f and 3g, the TEOF1s exhibit an S shape, notably different from the A-profiles, leading to significantly smaller correlations. We hypothesize that this is due to the competition between processes with different effects on the profile: these regions of low LNB (see Fig. 2a, blue shading) tend to have climatological descent, strongly varying cold SST, and a variety of cloud regimes (e.g., Stevens 2005; Neggers et al. 2007; Bony et al. 2015). Furthermore, the temperature in the boundary layer tends to be closely tied to SST while the temperature in the free troposphere can be strongly influenced by neighboring convective regions, as elaborated in our discussion of Fig. 4. Given these varying influences on temperature structure in the low-LNB regions, the leading vertical structure likely reflects a compromise among processes.

The A-profiles in Figs. 3a–f are not identical: as the value of LNB decreases, the conditionally averaged A-profile peak value decreases slightly from ~2.9 to 2.6 (the A-profiles in Figs. 3d–f overlap). For lower values of LNB in Fig. 3g, the A-profile shows a similar profile but has a notably smaller peak value ~2.2.

Figure 3i shows the variances explained by the TEOF1s as a function of p_{eof} (upper bin edge of LNB). For monthly data (blue), the explained variance is well above 50% for all p_{eof} cases, i.e., the corresponding TEOF1s indeed account for the majority of the tropospheric temperature variability. The explained variance at p_{eof} = 100 hPa is significantly lower because of the influence of the convective cold top. Also, the explained variance decreases with lower p_{eof}. In regions of lower LNB, the deep-convective temperature structure plays a slightly less dominant role, eventually becoming secondary for the lowest LNBs as in Figs. 3f and 3g.

For pentad (green) and daily (red) data, the temperatures are subject to higher frequency variation, resulting in lower but still reasonably high explained variance. Results from AIRS data show similar behavior but with even greater explained variance (>63% for monthly; Fig. S1 in the online supplemental material). Analysis of the Integrated Global Radiosonde Archive (IGRA; Durre et al. 2016) data from tropical sites also exhibits similar results (see Fig. S2 and Table S1). It suffices to say that the explained variance values presented here are all substantial, i.e., the TEOF1s are representative of the tropospheric temperature. Profiles of regression coefficient of tropospheric temperature onto temperature averaged over either [p_{cor}, 1000 hPa] or [p_{cor}, 850 hPa] at each level yield similar structures to the TEOF1s (not shown). The similarity of the regression, A-profile and TEOF1 for a wide range of LNB suggests that the A-profile reasonably approximates the tropospheric temperature perturbation structure over a considerable fraction of the tropics. We will elaborate further in the next section.

6. Geographical pattern of tropospheric temperature profile

We now turn to the geographical pattern of tropospheric temperature perturbation profile in the tropics. To compare the A-profiles with TEOF1s and examine how their relation varies geographically, Fig. 4 shows the vertical spatial correlation over [1000 hPa, p_{cor}] between the A-profile and TEOF1 at each location. The behavior as a function of the depth over which the comparison is made is also of interest. EOF analysis is thus recomputed across time dimension with a specified upper boundary p_{eof} and is compared with one single A-profile at the same location (using the mean averaged over the A-profiles computed using the monthly mean ERA-Interim and AIRS temperature data since the temporal variability of the tropical A-profile is small).

When the p_{eof} is sufficiently high (e.g., between 150 and 250 hPa in Figs. 4b–d,j–l), the vertical spatial correlation value tends to be substantial over most of the tropical ocean (indicated by red shadings), i.e., theoretical A-profile approximates the tropospheric temperature perturbation. Notably, the area of high correlation is much more extensive than that enclosed by the 5 mm day^{-1} precipitation contour, e.g., the latter region includes 23% of the total tropical oceanic grid points in contrast to 51% for ERA-Interim and 83% for AIRS with correlation exceeding 0.6 when p_{eof} = 250 hPa. Since the shape of A-profile does not vary much (as shown in Fig. 3), this implies that the leading mode of tropospheric temperature exhibits a broader pattern than that of heavy precipitation. For even higher p_{eof} (100 hPa in Figs. 4a,i), the robust feature of convective cold top of the TEOF1s modestly reduces the correlation. Low p_{eof} values (lower than 300 hPa in Figs. 4e–g,m–o) significantly reduces the correlation, e.g., over the Indian Ocean, partly because the TEOF1s tend to have a structure distinctly different from A-profiles at low levels (say as in Figs. 3f,g). It is also worth noting that, overall, the correlation is less sensitive to p_{eof} when AIRS data are used. The mean correlation as a function of p_{eof}, averaged over tropical ocean (blue) and over regions enclosed by the 5 mm day^{-1} precipitation contour (red), is summarized in Figs. 4h and 4p. The mean correlation averaged over heavily precipitating regions is consistently higher than that over the whole tropical ocean. The results computed using pentad and daily data exhibit similar patterns but with smaller correlations (not

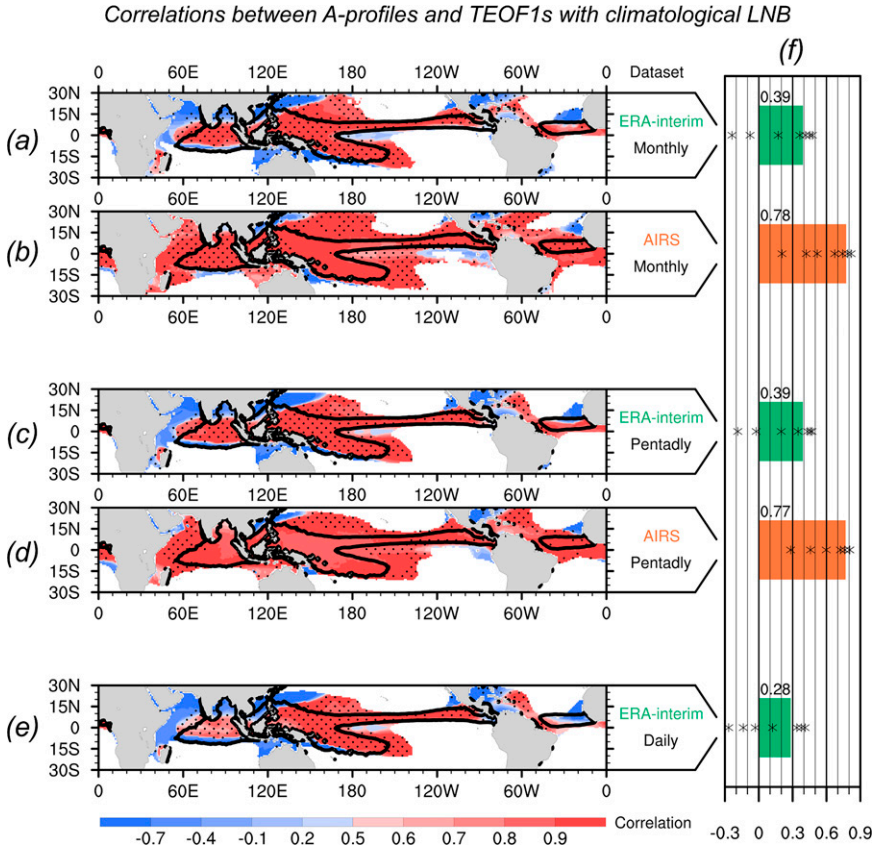

FIG. 5. (a) Vertical spatial correlations between the A-profile and TEOF1 computed with p_{eof} set to the climatological LNB at each grid point evaluated using ERA-Interim and AIRS at different time scales. Results from locations with climatological LNB $>$ 400 hPa are masked. Stippling indicates locations where the vertical spatial correlation is greater than at least four of the corresponding correlation values in Figs. 4a–g. (b) As in (a), but using AIRS monthly data, and stippling using Figs. 4i–o. (c),(d) As in (a) and (b), but using pentad data, and stippling using Figs. S3a–g and S3i–o. (e) As in (a), but using daily data, and stippling using Figs. S4a–g. (f) Mean vertical spatial correlations from (a) to (e) averaged over unmasked grid points (bars and values). The asterisks represent the mean vertical spatial correlations averaged over the same region as in (a)–(e) but computed with the prescribed p_{eof} values.

shown). As expected from WTG arguments, if we compute correlations only over the free troposphere [850 hPa, p_{cor}], the regions of low correlation in Fig. 4 over regions neighboring convection with cold SST, e.g., in the equatorial cold tongue, tend to be replaced by high correlation (see Fig. S4). In other words, the vertical profile in the free troposphere tends to reflect that of neighboring convective regions, but the boundary layer departs from this due to its connection to the underlying surface.

Figure 3 has demonstrated that the leading mode of tropospheric temperature perturbation depends on LNB. For sufficiently high LNB, the TEOF1 generally coincides with the A-profile, but the level at which convective cold top occurs varies with LNB. Thus, it makes sense to evaluate the correlation between the TEOF1 and A-profile over a range [p_{cor}, 1000 hPa] that is LNB dependent. This raises the question of how the geographical pattern of correlation between the TEOF1 and A-profile over the tropical ocean would be affected if, at each location, the TEOF1 is analyzed over a LNB-dependent domain in the vertical.

In Fig. 5a, the color shading shows the vertical spatial correlation between the TEOF1 and A-profile. Here, at each location, we compute the TEOF1 with p_{eof} chosen according to the climatological LNB (discretized as in Fig. 3) using ERA-Interim monthly data. The corresponding mean A-profile is also calculated, and the correlation is evaluated over [1000 hPa, p_{cor}] (as in Fig. 3). Only the results over regions with climatological LNB higher than 400 hPa are shown (low LNB and thus p_{eof} lead to small numbers of levels, causing insufficient sample size in the vertical for the computations of EOF and correlation). The 5 mm day^{-1} precipitation contour is shown for reference. Figures 5b–e show the same results but using data of different time scales and from the AIRS datasets. The average correlations over the displayed regions are summarized in Fig. 5f as bars (values indicated by texts).

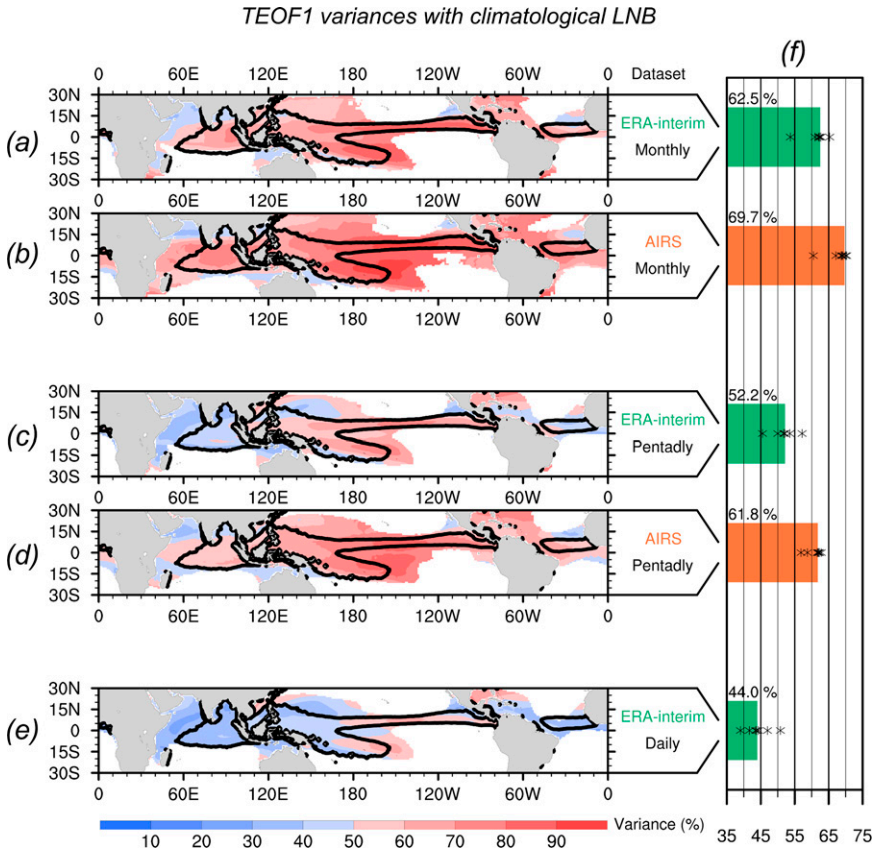

FIG. 6. As in Fig. 5, but for TEOF1 explained variance.

The color shading in Fig. 5a exhibits a pattern similar to that in Figs. 4a–e—not surprising given that the correlation in Fig. 4 tends to be robust to high enough p_{eof}. The average correlation over regions with climatological LNB exceeding 400 hPa (top bar in Fig. 5f) in comparison with the corresponding mean correlation in Figs. 4a–g averaged over the same domain (asterisks) demonstrates that the LNB-dependent method is a reasonable way to conduct the EOF analysis. That is, the LNB-dependent mean correlation exceeds most of the corresponding prescribed-p_{eof} mean correlations (Fig. 4), although smaller than the highest ones (for p_{eof} = 100–200 hPa). In Figs. 5a–e, the stippling indicates locations where the LNB-dependent correlation is greater than at least 4 out of 7 corresponding prescribed-p_{eof} correlations. If boundary layer (below 850 hPa) is excluded, mean correlations for both cases (LNB dependent and prescribed p_{eof}) would become even higher, e.g., 0.72 and 0.92 for ERA-Interim and AIRS monthly data (first two rows in Fig. 5f), respectively (not shown).

Correlation in Fig. 5b, computed using AIRS monthly data, tends to be higher than that in Fig. 5a, consistent with Fig. 4. Compared with Fig. 5a, the mean correlation here is notably higher, and is only smaller than two of the prescribed-p_{eof} cases (200 and 250 hPa). Note that the vertical structures between ERA-Interim and AIRS are quite similar (Fig. 3 versus Fig. S1). The difference in the correlation comes from additional variance in ERA-Interim from higher vertical wavenumber noise. It is not clear if this is part of the data assimilation process (Dee et al. 2011) or representation of real variance that is missed by the AIRS retrieval. In regions where AIRS exhibits low correlations, it tends to be due to a strong convective cold-top effect.

Figures 6a and 6b show the corresponding explained variance associated with the TEOF1 computed for Figs. 5a and 5b (and the corresponding mean explained variances are shown in Fig. 6f). Over the displayed regions, most locations have a high explained variance exceeding 50%, i.e., the TEOF1 dominates the tropospheric temperature variation. While the vertical spatial correlation is not sensitive to time scales (Figs. 5a,b compared with Figs. 5c–e), the explained variance in Fig. 6 tends to decrease for faster time scales due to greater explained variance not associated with the leading, convective-related structure. Such daily scale explained variance likely includes higher vertical mode gravity waves excited by convective heating variations and variations in the boundary layer relative to the free troposphere.

To summarize, the deep-convective temperature structure exhibits a broad pattern over the tropics. Furthermore, a high $p_{eof} \sim 200$ hPa helps capture the representative temperature structure that is approximated by the theoretical A-profile. On the other hand, climatological LNB provides an objective choice of p_{eof}. For high enough LNB, this results in leading temperature mode with reasonably high explained variance

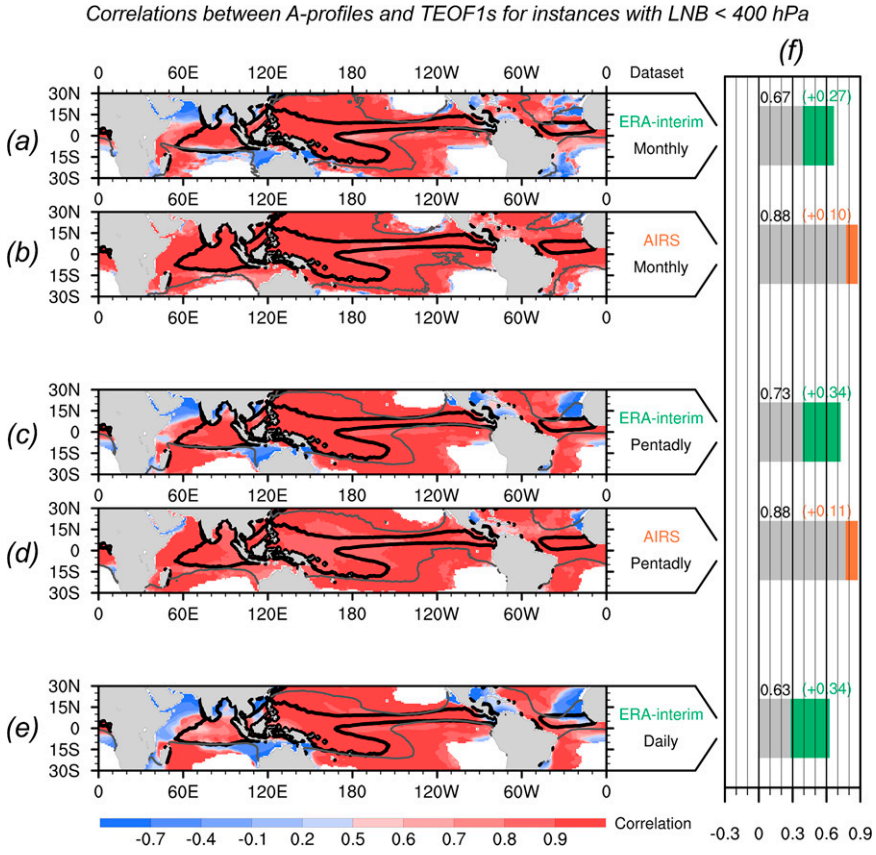

FIG. 7. As in Fig. 5, but the TEOF1 is computed using only instances with LNB < 400 hPa. The gray contours in (a)–(e) indicate climatological LNB = 400 hPa. Figure 5f is reproduced in (f) as gray bars (with numbers in black). The colored numbers denote the increase in the domain-averaged vertical spatial correlations.

and close to the A-profile. Longer time scales tend to have a higher fraction of variance explained by the profile. Compared with ERA-Interim, AIRS data tend to produce higher correlation and explained variance.

7. Temperature profile correlations excluding cases with low LNB

Despite the tropospheric temperature structure having a broad pattern in the tropics, one suspects that vertical spatial correlation between the leading temperature perturbation mode and A-profile is decreased by inclusion of conditions that are far from deep convection. This raises the question of whether excluding instances with low LNB in the EOF analysis can improve the correlation—in other words, using low LNB as an indicator of conditions for which a deep convective profile is less likely to be a good approximation. In Fig. 7, we repeat the analysis shown in Fig. 5, excluding the profiles with LNB lower than 400 hPa or missing LNB. The excluded profiles represent 46.4% of all profiles (27% with missing LNB); only 3.2% are between 750 and 400 hPa so the sensitivity to the choice of 400 hPa is modest.

The correlations in Figs. 7a–e over most of the tropical ocean are improved compared with Figs. 5a–e. This indicates that the low correlation in certain regions in Fig. 5 is the outcome of the TEOF1 being affected by low-LNB instances. The mean correlation over the displayed regions in Fig. 7f (color bars) show substantial increases compared with those in Fig. 5f (reproduced as gray bars in Fig. 7f; increments displayed as texts in the parentheses). The improvement is robust even at a daily time scale.

Off the coast of northwestern Australia and western Africa, and over the Arabian Sea, negative correlations can be noted in the ERA-Interim data. Dewpoint depression profiles conditioned on the correlation show that these regions are associated with dry lower troposphere (Fig. S3), impacting the conditional instability estimated via entraining plume calculations despite the high (nonentraining) LNB.

This analysis is not designed to directly address the spatial scale over which the WTG approximation holds, but the comparison between Figs. 4 and 7 does suggest some inferences on this. In Fig. 4, the correlations tend to decrease away from the convection zones on scales of some tens of degrees of longitude, suggesting that weak temperature gradient constraints do not hold well across the scale of the descent regions in the eastern Pacific. In contrast, when using only conditions where deep convection tends to occur reasonably often, as in Fig. 7, high correlation can extend across portions of these regions. Analysis to address scales of

validity of WTG would be of interest, but would require additional hypotheses beyond the scope of this study. Specifically, it would require a way of constructing a hypothesized CQE + WTG temperature profile in the free troposphere of a given nonconvecting region, based on profiles of neighboring convective regions.

8. Discussion and conclusions

In convective quasi-equilibrium theory, tropical tropospheric temperature perturbations are expected to follow vertical profiles constrained by convection. This is based on assumptions that a conditionally unstable profile will tend to be adjusted toward a profile that yields small buoyancy for convectively raised parcels, and that gravity wave adjustment communicates this across large horizontal scales in the tropics. This leads to the tropical tropospheric temperature exhibiting a pattern broader than that of precipitation, i.e., occurrence of deep convection. The vertical structure of perturbations to these convective profiles are referred to as A-profiles. In general, these should include the effect of entrainment, but they have commonly been approximated by perturbations of moist pseudoadiabats, either for parcels raised from the boundary layer or by MSE-conserving parcels perturbed from the basic state temperature profile.

Given the strong evidence for the importance of entrainment in the operation of convection, the first question we address is how this impacts the temperature profile perturbations characteristic of convection. Comparing the latter idealized A-profile and temperature perturbations derived from entraining and nonentraining parcel computations, differences are found to be modest under convective conditions. This is because the lower troposphere tends to be close to saturation under these conditions, so entrainment has only a modest impact on convective plume temperature. Thus, the pseudoadiabatic perturbations about the observed profile provide useful baseline A-profiles to compare to observations. The typical A-profile increases from unity near the surfaces to its peak value ~2.7 around 225 hPa, and decreases with further increase of height.

The leading mode of temperature variation indeed tends to exhibit substantial similarity to the theoretical A-profile over most of the tropics. This applies over regions that extend beyond the convection zones, as expected, although there are certain exceptions. The level of neutral buoyancy (LNB) is used as a measure of the depth of convection—estimated by the height through which a nonentraining parcel would be conditionally unstable by comparing the surface value of MSE with the environment saturation MSE profile. When conditioned on the LNB, the A-profile does not vary significantly. However, the leading mode of tropospheric temperature variation is more sensitive. For climatological LNB higher than 400 hPa, the leading mode tends to coincide with the A-profile, but significant deviations can be noted near the LNB. Here the observed temperature perturbations decrease rapidly and go negative. This effect, known as the convective cold top, has been previously suggested to occur due to dynamical effects, with vertical velocity generating negative temperature perturbations of amplitude necessary to cancel pressure gradients above the convection (Holloway and Neelin 2007). These features are robust across all the time scales (monthly, pentad, daily).

By excluding the instances with LNB lower than 400 hPa from the analysis, the vertical spatial correlation between the leading tropospheric temperature mode and the A-profile significantly increases throughout the tropics. Lower free tropospheric humidity can impact the occurrence of deep convection via entrainment (Tompkins 2001; Bretherton et al. 2004; Zhang 2009; Ahmed and Neelin 2021), thus yielding low correlations, even over certain regions with high nonentraining LNB, e.g., over the Arabian Sea and off the coast of northwestern Australia and west Africa. This is consistent with the rare occurrence of deep convection and low precipitation in these regions (Peng et al. 2014; Houze et al. 2015; Taszarek et al. 2021).

Overall, the results are consistent with temperature perturbations exhibiting a vertical structure consistent with convective constraints over much of the tropics, for regions where convection is expected to occur or in the immediate neighborhood of these. The clear exception is that near the top of the layer that might be expected to undergo conditional instability, the convective profile gives way to a characteristic convective cold-top effect. This is postulated to be a dynamical effect in which vertical velocity above the heating drives reduction in buoyancy and negative temperature perturbations to balance baroclinic pressure gradients created within the heating region. Given that this is here seen empirically to be a widely repeatable effect of convection on the temperature structure, convective quasi-equilibrium theory should be adapted to account for this modification. The question of why profiles based on moist adiabatic considerations work reasonably well given that entrainment in the lower troposphere is important to the onset of convective instability is suggested here to have a simple resolution. Entraining and nonentraining assumptions result in similar leading temperature mode because the lower free troposphere tends to be close to saturation when strong convection occurs, limiting the impact of environment humidity on plume temperature through entrainment. In other words, the impact of entrainment is primarily to create a requirement of high lower-tropospheric relative humidity before deep convection can occur, rather than to greatly modify the vertical structure of temperature perturbations associated with the deep convection.

Acknowledgments. The authors thank Dr. Fiaz Ahmed at UCLA and Dr. Hien Bui at Pusan National University for helpful discussions. Dr. Ahmed provided the code package for entraining plume computations. YXL and JYY are supported by the Ministry of Science and Technology (MOST) of Taiwan through Grants 108-2111-M-008-038 and 109-2111-M-008-010. YXL was also supported by the MOST Overseas Research Project 109-2917-I-008-003 for the period of March 2020 through March 2021. JDN and YHK were supported by National Science Foundation (NSF) Grant AGS-1936810 and National Atmospheric and Oceanic Administration (NOAA) Grant NA21OAR4310354. The insightful reviews by three anonymous reviewers are greatly appreciated.

Data availability statement. The ERA-Interim data used in this study are openly available at https://apps.ecmwf.int/datasets/, and the AIRS satellite data at https://doi.org/10.5067/Aqua/AIRS/DATA301 and https://doi.org/10.5067/Aqua/AIRS/DATA319. Additional Integrated Global Radiosonde Archive (IGRA) sounding data from https://www.ncdc.noaa.gov/data-access/weather-balloon/integrated-global-radiosonde-archive are used for producing Fig. S2 in the supplementary materials.

REFERENCES

Adames, Á. F., S. W. Powell, F. Ahmed, V. C. Mayta, and J. D. Neelin, 2021: Tropical precipitation evolution in a buoyancy-budget framework. *J. Atmos. Sci.*, **78**, 509–528, https://doi.org/10.1175/JAS-D-20-0074.1.

Ahmed, F., and J. D. Neelin, 2018: Reverse engineering the tropical precipitation–buoyancy relationship. *J. Atmos. Sci.*, **75**, 1587–1608, https://doi.org/10.1175/JAS-D-17-0333.1.

——, and ——, 2021: Protected convection as a metric of dry air influence on precipitation. *J. Climate*, **34**, 3821–3838, https://doi.org/10.1175/JCLI-D-20-0384.1.

AIRS Science Team and J. Teixeira, 2013a: AIRS/Aqua L3 monthly standard physical retrieval (AIRS+AMSU) 1 degree × 1 degree, version 006 (AIRX3STM). GES DISC, accessed 2 August 2018, https://doi.org/10.5067/Aqua/AIRS/DATA319.

—— and ——, 2013b: AIRS/Aqua L3 daily standard physical retrieval (AIRS+AMSU) 1 degree × 1 degree, version 006 (AIRX3STD). GES DISC, accessed 2 August 2018, https://doi.org/10.5067/Aqua/AIRS/DATA301.

—— and ——, 2013c: AIRS/Aqua L3 monthly support product (AIRS+AMSU) 1 degree × 1 degree, version 006 (AIRX3SPM). GES DISC, accessed 2 July 2021, https://doi.org/10.5067/Aqua/AIRS/DATA322.

—— and ——, 2013d: AIRS/Aqua L3 daily support product (AIRS+AMSU) 1 degree × 1 degree, version 006 (AIRX3SPD). GES DISC, accessed 2 July 2021, https://doi.org/10.5067/Aqua/AIRS/DATA304.

Arakawa, A., 2004: The cumulus parameterization problem: Past, present, and future. *J. Climate*, **17**, 2493–2525, https://doi.org/10.1175/1520-0442(2004)017<2493:RATCPP>2.0.CO;2.

——, and W. H. Schubert, 1974: Interaction of a cumulus cloud ensemble with the large-scale environment, part I. *J. Atmos. Sci.*, **31**, 674–701, https://doi.org/10.1175/1520-0469(1974)031<0674:IOACCE>2.0.CO;2.

Betts, A. K., 1982: Saturation point analysis of moist convective overturning. *J. Atmos. Sci.*, **39**, 1484–1505, https://doi.org/10.1175/1520-0469(1982)039<1484:SPAOMC>2.0.CO;2.

——, 1986: A new convective adjustment scheme. Part I: Observational and theoretical basis. *Quart. J. Roy. Meteor. Soc.*, **112**, 677–691, https://doi.org/10.1002/qj.49711247307.

Bony, S., and Coauthors, 2015: Clouds, circulation and climate sensitivity. *Nat. Geosci.*, **8**, 261–268, https://doi.org/10.1038/ngeo2398.

Bretherton, C. S., and A. H. Sobel, 2003: The Gill model and the weak temperature gradient approximation. *J. Atmos. Sci.*, **60**, 451–460, https://doi.org/10.1175/1520-0469(2003)060<0451:TGMATW>2.0.CO;2.

——, M. E. Peters, and L. E. Back, 2004: Relationships between water vapor path and precipitation over the tropical oceans. *J. Climate*, **17**, 1517–1528, https://doi.org/10.1175/1520-0442(2004)017<1517:RBWVPA>2.0.CO;2.

Brown, R. G., and C. S. Bretherton, 1997: A test of the strict quasi-equilibrium theory on long time and space scales. *J. Atmos. Sci.*, **54**, 624–638, https://doi.org/10.1175/1520-0469(1997)054<0624:ATOTSQ>2.0.CO;2.

Dee, D. P., and Coauthors, 2011: The ERA-Interim reanalysis: Configuration and performance of the data assimilation system. *Quart. J. Roy. Meteor. Soc.*, **137**, 553–597, https://doi.org/10.1002/qj.828.

Derbyshire, S. H., I. Beau, P. Bechtold, J.-Y. Gandpeix, J.-M. Piriou, J.-L. Redelsperger, and P. Soares, 2004: Sensitivity of moist convection to environmental humidity. *Quart. J. Roy. Meteor. Soc.*, **130**, 3055–3079, https://doi.org/10.1256/qj.03.130.

Durre, I., X. Yin, S. Applequist, J. Arnfield, and R. S. Vose, 2016: Integrated Global Radiosonde Archive (IGRA), version 2. NOAA/National Centers for Environmental Information, accessed 29 August 2018, https://doi.org/10.7289/V5X63K0Q.

Emanuel, K. A., J. D. Neelin, and C. S. Bretherton, 1994: On large-scale circulations in convecting atmospheres. *Quart. J. Roy. Meteor. Soc.*, **120**, 1111–1143, https://doi.org/10.1002/qj.49712051902.

Fueglistaler, S., C. Radley, and I. M. Held, 2015: The distribution of precipitation and the spread in tropical upper tropospheric temperature trends in CMIP5/AMIP simulations. *Geophys. Res. Lett.*, **42**, 6000–6007, https://doi.org/10.1002/2015GL064966.

Holloway, C. E., and J. D. Neelin, 2007: The convective cold top and quasi equilibrium. *J. Atmos. Sci.*, **64**, 1467–1487, https://doi.org/10.1175/JAS3907.1.

——, and ——, 2009: Moisture vertical structure, column water vapor, and tropical deep convection. *J. Atmos. Sci.*, **66**, 1665–1683, https://doi.org/10.1175/2008JAS2806.1.

——, and ——, 2010: Temporal relations of column water vapor and tropical precipitation. *J. Atmos. Sci.*, **67**, 1091–1105, https://doi.org/10.1175/2009JAS3284.1.

Houze, R. A., Jr., K. L. Rasmussen, M. D. Zuluaga, and S. R. Brodzik, 2015: The variable nature of convection in the tropics and subtropics: A legacy of 16 years of the Tropical Rainfall Measuring Mission satellite. *Rev. Geophys.*, **53**, 994–1021, https://doi.org/10.1002/2015RG000488.

Huffman, G. J., and Coauthors, 2007: The TRMM Multisatellite Precipitation Analysis (TMPA): Quasi-global, multiyear, combined-sensor precipitation estimates at fine scales. *J. Hydrometeor.*, **8**, 38–55, https://doi.org/10.1175/JHM560.1.

——, R. F. Adler, D. T. Bolvin, and E. J. Nelkin, 2010: The TRMM Multi-Satellite Precipitation Analysis (TMPA). *Satellite Rainfall Applications for Surface Hydrology*, Springer, 3–22, https://doi.org/10.1007/978-90-481-2915-7_1.

Kuang, Z., 2008: Modeling the interaction between cumulus convection and linear gravity waves using a limited-domain cloud system–resolving model. *J. Atmos. Sci.*, **65**, 576–591, https://doi.org/10.1175/2007JAS2399.1.

Kuo, H. L., 1974: Further studies of the parameterization of the influence of cumulus convection on large-scale flow. *J. Atmos. Sci.*, **31**, 1232–1240, https://doi.org/10.1175/1520-0469(1974)031<1232:FSOTPO>2.0.CO;2.

Kuo, Y.-H., J. D. Neelin, and C. R. Mechoso, 2017: Tropical convective transition statistics and causality in the water vapor–precipitation relation. *J. Atmos. Sci.*, **74**, 915–931, https://doi.org/10.1175/JAS-D-16-0182.1.

——, K. A. Schiro, and J. D. Neelin, 2018: Convective transition statistics over tropical oceans for climate model diagnostics: Observational baseline. *J. Atmos. Sci.*, **75**, 1553–1570, https://doi.org/10.1175/JAS-D-17-0287.1.

Lin, J.-L., T. Qian, T. Shinoda, and S. Li, 2015: Is the tropical atmosphere in convective quasi-equilibrium? *J. Climate*, **28**, 4357–4372, https://doi.org/10.1175/JCLI-D-14-00681.1.

Manabe, S., J. S. Smagorinsky, and R. F. Strickler, 1965: Simulated climatology of a general circulation model with a hydrological cycle. *Mon. Wea. Rev.*, **93**, 769–798, https://doi.org/10.1175/1520-0493(1965)093<0769:SCOAGC>2.3.CO;2.

Neelin, J. D., and I. M. Held, 1987: Modeling tropical convergence based on the moist static energy budget. *Mon. Wea. Rev.*, **115**, 3–12, https://doi.org/10.1175/1520-0493(1987)115<0003:MTCBOT>2.0.CO;2.

——, and J.-Y. Yu, 1994: Modes of tropical variability under convective adjustment and the Madden–Julian oscillation. Part I: Analytical theory. *J. Atmos. Sci.*, **51**, 1876–1894, https://doi.org/10.1175/1520-0469(1994)051<1876:MOTVUC>2.0.CO;2.

——, and N. Zeng, 2000: A quasi-equilibrium tropical circulation model—Formulation. *J. Atmos. Sci.*, **57**, 1741–1766, https://doi.org/10.1175/1520-0469(2000)057<1741:AQETCM>2.0.CO;2.

——, O. Peters, J. W.-B. Lin, K. Hales, and C. E. Holloway, 2008: Rethinking convective quasi-equilibrium: Observational constraints for stochastic convective schemes in climate models. *Philos. Trans. Roy. Soc.*, **366**, 2579–2602, https://doi.org/10.1098/rsta.2008.0056.

Neggers, R. A. J., J. D. Neelin, and B. Stevens, 2007: Impact mechanisms of shallow cumulus convection on tropical climate dynamics. *J. Climate*, **20**, 2623–2642, https://doi.org/10.1175/JCLI4079.1.

Nie, J., W. R. Boos, and Z. Kuang, 2010: Observational evaluation of a convective quasi-equilibrium view of monsoons. *J. Climate*, **23**, 4416–4428, https://doi.org/10.1175/2010JCLI3505.1.

O'Gorman, P. A., and M. S. Singh, 2013: Vertical structure of warming consistent with an upward shift in the middle and upper troposphere. *Geophys. Res. Lett.*, **40**, 1838–1842, https://doi.org/10.1002/grl.50328.

Peng, J., H. Zhang, and Z. Li, 2014: Temporal and spatial variations of global deep cloud systems based on CloudSat and CALIPSO satellite observations. *Adv. Atmos. Sci.*, **31**, 593–603, https://doi.org/10.1007/s00376-013-3055-6.

Raymond, D. J., and M. J. Herman, 2011: Convective quasi-equilibrium reconsidered. *J. Adv. Model. Earth Syst.*, **3**, M08003, https://doi.org/10.1029/2011MS000079.

Sahany, S., J. D. Neelin, K. Hales, and R. B. Neale, 2012: Temperature–moisture dependence of the deep convective transition as a constraint on entrainment in climate models. *J. Atmos. Sci.*, **69**, 1340–1358, https://doi.org/10.1175/JAS-D-11-0164.1.

Santer, B. D., and Coauthors, 2005: Amplification of surface temperature trends and variability in the tropical atmosphere. *Science*, **309**, 1551–1556, https://doi.org/10.1126/science.1114867.

Savazzi, A. C. M., C. Jakob, and A. P. Siebesma, 2021: Convective mass-flux from long term radar reflectivities over Darwin, Australia. *J. Geophys. Res. Atmos.*, **126**, e2021JD034910, https://doi.org/10.1029/2021JD034910.

Schiro, K. A., F. Ahmed, S. E. Giangrande, and J. D. Neelin, 2018: GoAmazon2014/5 campaign points to deep-inflow approach to deep convection across scales. *Proc. Natl. Acad. Sci. USA*, **115**, 4577–4582, https://doi.org/10.1073/pnas.1719842115.

Siebesma, A. P., and Coauthors, 2003: A large eddy simulation intercomparison study of shallow cumulus convection. *J. Atmos. Sci.*, **60**, 1201–1219, https://doi.org/10.1175/1520-0469(2003)60<1201:ALESIS>2.0.CO;2.

Singh, M. S., and P. A. O'Gorman, 2013: Influence of entrainment on the thermal stratification in simulations of radiative-convective equilibrium. *Geophys. Res. Lett.*, **40**, 4398–4403, https://doi.org/10.1002/grl.50796.

——, R. A. Warren, and C. Jakob, 2019: A steady-state model for the relationship between humidity, instability, and precipitation in the tropics. *J. Adv. Model. Earth Syst.*, **11**, 3973–3994, https://doi.org/10.1029/2019MS001686.

Sobel, A. H., and J. D. Neelin, 2006: The boundary layer contribution to intertropical convergence zones in the quasi-equilibrium tropical circulation model framework. *Theor. Comput. Fluid Dyn.*, **20**, 323–350, https://doi.org/10.1007/s00162-006-0033-y.

——, J. Nilsson, and L. M. Polvani, 2001: The weak temperature gradient approximation and balanced tropical moisture waves. *J. Atmos. Sci.*, **58**, 3650–3665, https://doi.org/10.1175/1520-0469(2001)058<3650:TWTGAA>2.0.CO;2.

Steiner, A. K., and Coauthors, 2020: Observed temperature changes in the troposphere and stratosphere from 1979 to 2018. *J. Climate*, **33**, 8165–8194, https://doi.org/10.1175/JCLI-D-19-0998.1.

Stevens, B., 2005: Atmospheric moist convection. *Annu. Rev. Earth Planet. Sci.*, **33**, 605–643, https://doi.org/10.1146/annurev.earth.33.092203.122658.

Taszarek, M., J. T. Allen, M. Marchio, and H. E. Brooks, 2021: Global climatology and trends in convective environments from ERA5 and rawinsonde data. *npj Climate Atmos.*, **4**, 35, https://doi.org/10.1038/s41612-021-00190-x.

Tompkins, A. M., 2001: Organization of tropical convection in low vertical wind shears: The role of water vapor. *J. Atmos. Sci.*, **58**, 529–545, https://doi.org/10.1175/1520-0469(2001)058<0529:OOTCIL>2.0.CO;2.

Xu, K.-M., and K. A. Emanuel, 1989: Is the tropical atmosphere conditionally unstable? *Mon. Wea. Rev.*, **117**, 1471–1479, https://doi.org/10.1175/1520-0493(1989)117<1471:ITTACU>2.0.CO;2.

Yano, J.-I., and R. S. Plant, 2012: Convective quasi-equilibrium. *Rev. Geophys.*, **50**, RG4004, https://doi.org/10.1029/2011RG000378.

——, and ——, 2016: Generalized convective quasi-equilibrium principle. *Dyn. Atmos. Oceans*, **73**, 10–33, https://doi.org/10.1016/j.dynatmoce.2015.11.001.

Yu, J.-Y., and J. D. Neelin, 1997: Analytic approximations for moist convectively adjusted regions. *J. Atmos. Sci.*, **54**, 1054–1063, https://doi.org/10.1175/1520-0469(1997)054<1054:AAFMCA>2.0.CO;2.

Zhang, G. J., 2009: Effects of entrainment on convective available potential energy and closure assumptions in convection parameterization. *J. Geophys. Res.*, **114**, D07109, https://doi.org/10.1029/2008JD010976.